A Deep Learning with Metaheuristic Optimization-Driven Breast Cancer Segmentation and Classification Model using Mammogram Imaging

M. Sreevani
Department of Computer Science, St. Peter's Institute of Higher Education and Research, Chennai, India | Department of Computer Science and Engineering, Vemu Institute of Technology, Chittoor, India
vani.cse183@gmail.com (corresponding author missing)

R. Latha
Department of Computer Applications, St. Peter's Institute of Higher Education and Research, Chennai, India
latharamavel1212@gmail.com

Received: 25 October 2024 | Revised: 14 November 2024, 6 December 2024, 9 December 2024, and 16 December 2024 | Accepted: 18 December 2024

 DOI: https://doi.org/10.48084/etasr.9406

ABSTRACT

Cancer is the second leading cause of death globally, with Breast Cancer (BC) accounting for 20% of the new diagnoses, making it a major cause of morbidity and mortality. Mammography is effective for BC detection, but lesion interpretation is challenging, prompting the development of Computer-Aided Diagnosis (CAD) systems to assist in lesion classification and detection. Machine Learning (ML) and Deep Learning (DL) models are widely used in disease diagnosis. Therefore, this study presents an Optimized Graph Convolutional Recurrent Neural Network based Segmentation for Breast Cancer Recognition and Classification (OGCRNN-SBCRC) technique. In the preparation phase, images and masks are annotated and then classified as benign or malignant. To achieve this, the Wiener Filter (WF)-based noise removal and log transform-based contrast enhancement are used for preprocessing. The OGCRNN-SBCRC technique utilizes the UNet++ method for segmentation and the RMSProp optimizer for parameter tuning. In addition, the OGCRNN-SBCRC technique employs the ConvNeXtTiny Convolution Neural Network (CNN) approach for feature extraction. For BC classification and detection, the Graph Convolutional Recurrent Neural Network (GCRNN) model is used. Finally, the Aquila Optimizer (AO) model is employed for the hyperparameter tuning of the GCRNN approach. The simulation analysis of the OGCRNN-SBCRC methodology, using the BC image dataset, demonstrated superior performance with an accuracy of 99.65%, surpassing existing models.

Keywords-deep learning; breast cancer; segmentation; mammogram imaging; aquila optimizer

I. INTRODUCTION

Cancer is a major public health problem in the world today. According to the World Health Organization (WHO), 8.2 million deaths were caused by cancer in 2012, and 27 million new cases are predicted to have occurred by 2030 [1]. BC, the most common cancer in women with a high mortality rate, originates in the breast glands and is surrounded by ducts, connective tissue, lymph nodes, nerves, and blood vessels [2]. BC can develop in various parts of the breast, with more than 20 recognized types. The most common type is ductal carcinoma [3]. BC cells are typically identified by geometric shapes, such as architectural distortions, microcalcifications, and masses [4]. Early detection and treatment can significantly reduce the mortality rate [5].

Mammography, which uses lower doses of x-rays to visualize the inner breast structures, is the preferred technique for identifying BC [6]. Modern mammograms use less radiation and are crucial for early BC detection, effectively identifying tumors and calcifications [7]. Researchers have used techniques, such as grey level co-occurrence matrices, shape properties, and local binary patterns to classify mammogram images based on local and global texture information [8]. Recently, ML and DL models have shown major advancements in computer vision, particularly in areas like object classification and detection, and are increasingly

applied in medical imaging for tissue classification in mammogram analysis [9].

This study presents an OGCRNN-SBCRC technique. In the preparation phase, images and masks are annotated and then classified as benign or malignant. To achieve this, WF-based noise removal and log transform-based contrast enhancement are used for preprocessing. The OGCRNN-SBCRC technique utilizes the UNet++ method for segmentation and the RMSProp optimizer for parameter tuning. In addition, the OGCRNN-SBCRC technique employs the ConvNeXtTiny CNN approach for feature extraction. For BC classification and detection, the GCRNN model is used. Finally, the AO model is used for the hyperparameter tuning of the GCRNN approach. The key contribution of the OGCRNN-SBCRC model is given below.

- The WF model improves image quality by removing noise and using log transformation for contrast enhancement. These methods contribute to better preprocessing, resulting in improved performance.
- The UNet++ ensures accurate segmentation with multi-scale pathways for better tumor delineation, whereas the GCRNN improves BC detection and classification by capturing spatial relationships for more precise predictions.
- The AO is used to effectively tune hyperparameters improving model performance by finding the optimal configuration for improved accuracy and robustness in BC detection and segmentation.
- The novelty lies in the integration of advanced noise removal, contrast enhancement, and cutting-edge architectures with AO for hyperparameter tuning, resulting in a unified and highly effective approach for BC detection and segmentation.

II. LITERATURE REVIEW

Authors in [10] presented a DL-based ensemble classifier by integrating Transfer Learning (TL) methods, such as MobileNet-V2, ResNet, and AlexNet, with residual learning and depthwise separable convolution. Authors in [11] utilized dual techniques and Otsu threshold models. Authors in [12] focused on enhancing an optimizer-based classification method, utilizing Adaptive Histogram Equalization (AHE) and Gaussian Filtering (GF) for preprocessing, and Markov Random Adaptive Segmentation (MRAS) for boundary detection. Authors in [13], developed an Adaptive Fuzzy C-Means Segmentation and Deep CNN (AFCM-DCNN) by utilizing the Grey Code Approximation Pre-processing (GCAP) model. Authors in [14] introduced a dual CNN structure with Bayesian Optimization (BO) for hyperparameter initialization, designed as 3-Residual Blocks CNN and 2-Residual Blocks CNN.

Authors in [15] presented a DL-based technique and authors in [16] presented a technique incorporating ensemble DL and advanced TL. Authors in [17] proposed a self-attention Deep CNN (DCNN) enhanced with Smack Echolocation Optimization (SELO) for classification and a SELO-mask Region-based CNN (RCNN) for segmentation. Authors in [18] developed a CNN model that was optimized with the Particle Swarm Optimization (PSO) method. Authors in [19] proposed a model using VGG16 for feature extraction, whale optimization for selection, and Grey Wolf Optimizer (GWO) with k-NN for classification. Authors in [20] proposed an Adam Golden Search Optimization-based DCNN (AGSO-DCNN) method using GF-based preprocessing, k-means clustering for segmentation, and Local Vector Patterns (LVP) and Pyramid Histogram of Oriented Gradients (PHOG) for feature extraction.

III. PROPOSED METHOD

This study presents an OGCRNN-SBCRC technique using mammogram imaging. The preparation phase includes the processes of pre-processing, segmentation, feature extraction, classification, and hyperparameter tuning. Figure 1 represents the overall flow of the OGCRNN-SBCRC method.

A. Preprocessing Stage

The OGCRNN-SBCRC technique employs a two-stage preprocessing approach, WF-based noise removal, and log transform-based contrast enhancement [21]:

- Noise removal using WF: The WF is a great image pre-processing model commonly deployed in medical imaging, mainly to improve mammograms in the detection of BC. The WF reduces noise while preserving important image details, improving tissue visualization and assisting radiologists in tumor detection, thereby improving the diagnostic accuracy of BC.
- Contrast enhancement using log transformation: Log transform-based contrast enhancement is a model utilized to enhance the visibility of regions in BC images, primarily in mammograms. Applying a logarithmic function to pixel intensity improves the range of darker pixels, making low-intensity features more distinct and enhancing the visualization of cancerous areas or microcalcifications in the breast tissue for early detection. The log transformation is given by:

$$s = c \cdot log(1 + r) \quad (1)$$

where s represents the output pixel intensities, r represents the input pixel intensities, and c is a scaling constant that enhances contrast in low-intensity areas highlighting BC image patterns.

B. Segmentation Process

For the segmentation process, the OGCRNN-SBCRC model is implemented using the UNet++ architecture [22]. UNet++ enhances the original UNet with a more complex, hierarchical structure that includes stacked skip pathways, multiple encoding feature maps, layered decoding skip connections, and an aggregation path for enhanced multi-scale feature representation.

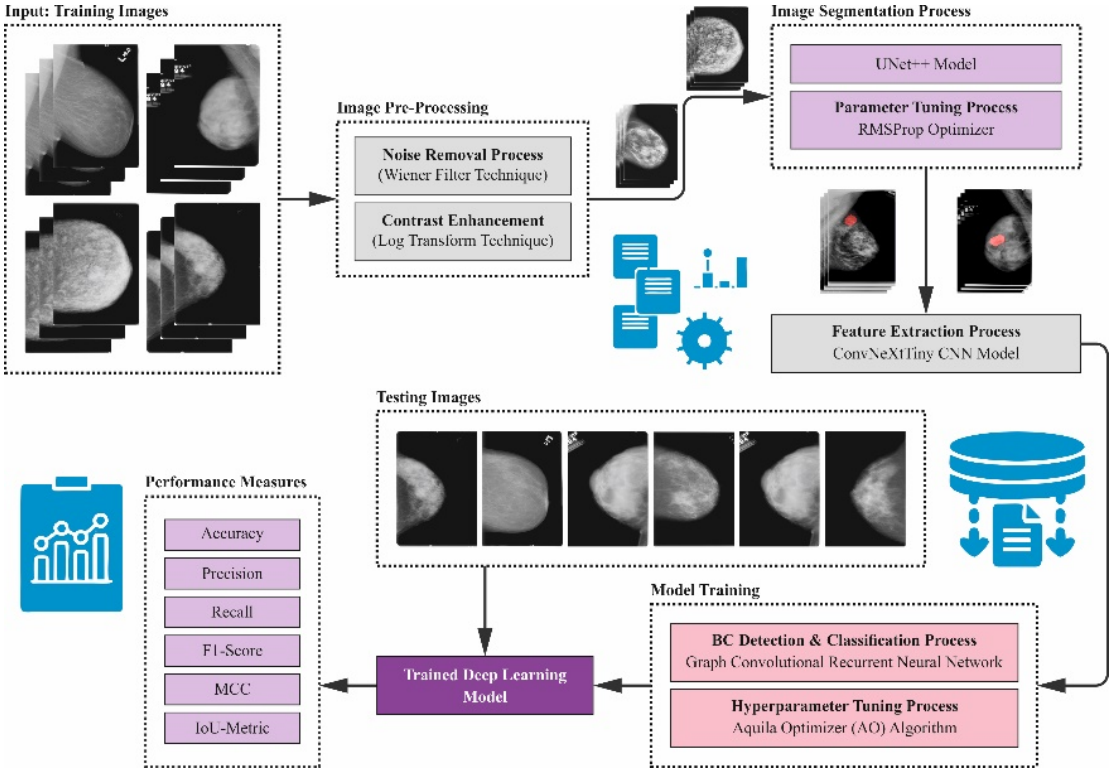

Fig. 1. Overall workflow of the OGCRNN-SBCRC method.

Parameter tuning is performed deploying the RMSProp optimizer [23]. The RMSprop optimizer stabilizes vertical variations and accelerates convergence by using a momentum, typically set to $\beta = 0.95\,(1-\beta = 0.005)$, and a learning rate $\alpha = 0.001$, to optimize the model fitting process. When applying this optimizer during backpropagation, the bias β and the weight W are modified by (2) and (3), where Vdw and Vdb denote specific values derived from (4) and (5), respectively, and are used to reduce the loss. dw denotes the weighted derivative and db represents the derivative concerning the loss. ε denotes a non-zero value that is integrated to safeguard the method from important errors regarding zero values for $\sqrt{vdw}$ and $\sqrt{vdb}$.

$$W = W_{t-1} - \alpha * \frac{dw}{\sqrt{vdw}-\varepsilon} \quad (2)$$

$$b = b_{t-1} - \alpha * \frac{db}{\sqrt{vdb}-\varepsilon} \quad (3)$$

$$Vdw = \beta * Vdw + (1-\beta) * dw^2 \quad (4)$$

$$Vdb = \beta * Vdb + (1-\beta) * db^2 \quad (5)$$

C. Feature Extraction Method

In addition, the OGCRNN-SBCRC technique utilizes the ConvNeXtTiny CNN model for feature extraction [24]. ResNet-based CNNs have been widely employed for object detection due to the advantages of weight sharing and translation. To balance detection accuracy and speed, the tiny version of ConvNeXt is used in the present study.

D. Classification Model

The GCRNN model is utilized for BC classification and detection [25]. Convolutional operations are key in ML, especially in CNNs, which outperform in image classification by processing multidimensional arrays. While CNNs focus on Euclidean structures, Graph Convolutional Networks (GCNs) adapt these operations to graph data, enabling effective node feature extraction from graph models. The output of a GCN method is typically computed as:

$$Y = \tilde{A}XW \quad (6)$$

where, X represents the input data, Y represents the output, and W is the parameter matrix of the model. Additionally, $\tilde{A}$ is the regularized adjacency matrix, which can be read as:

$$\tilde{A} = (\hat{D}^{-\frac{1}{2}}\hat{A}\hat{D}^{-\frac{1}{2}}) \quad (7)$$

with $\hat{A} = A + I$, and where A is the adjacency matrix build upon the graph in which the links represent the correlation between the different time series, I is the identity matrix, and $\hat{D}$ is the diagonal degree matrix of $\hat{A}$. A Recurrent Neural Network (RNN) predicts outcomes by using both input data and outputs from neighboring units, processing temporal data through connections that exploit previous states, particularly within the Hidden Layer (HL). Here, $x = (x_1, \ldots, x_t)$ is the input sequence, $y = (y_1, \ldots, y_t)$ is the output sequence, and $h^n = (h_1^n, \ldots, h_t^n)$ represents the hidden vectors in layer n. Based on this, the overall hidden state h_t of the initial layer is computed as:

$$h_t^1 = \tanh(W_{xh^1}x_t + W_{h^1h^1}h_{t-1}^1 + b_h^1) \quad (8)$$

where W denotes the weighted matrix, W_{xh^1} denotes the weights of the connection between the primary input and the hidden layer, whereas $W_{h^1h^1}$ denotes the recurrent link weights in the initial HL and b_h^1 denotes the bias. The hidden states of the layer n are computed as:

$$h_t^n = \tanh(W_{h^{n-1}h^n}h_t^{n-1} + W_{h^nh^n}h_{t-1}^n + b_h^n) \quad (9)$$

where $W_{h^{n-1}h^n}$ represents the weight assigned to the connection between the n and $n-1$ layers, $W_{h^nh^n}$ represents the weight assigned to the recurrent connection of the n-th layer, and $b_{h_t}^n$ is the relative bias. The temporal output representation from the RNN is given by:

$$y_t = W_{h^ny}h_t^n + b_y \quad (10)$$

where W_{h^ny} is the weight assigned to the connection between the output layer and the n layer and b_y is the bias. The basic recurrent units can suffer from the vanishing gradient problem, limiting the learning of long-term dependencies. To address this problem, Long Short-Term Memory (LSTM) units were introduced, with modified hidden state calculations, whereas (8-10) are still applicable.

$$f_t = \sigma\left(W_f h_{t-1}^n + w_f h_t^{n-1} + b_f\right) \quad (11)$$

$$i_t = \sigma\left(W_i h_{t-1}^n + w_j h_t^{n-1} + b_i\right) \quad (12)$$

$$C_t = f_t C_{t-1} + i_t \tanh(W_c h_{t-1}^n + w_c h_t^{n-1} + b_c) \quad (13)$$

$$o_t = \sigma(W_o h_{t-1}^n + w_o h_t^{n-1} + b_o) \quad (14)$$

$$h_t = o_t \tanh(C_t) \quad (15)$$

where the adopted activation functions for the gates are represented by the sigmoid (σ) and the hyperbolic tangent ($\tanh$). The states of the output, forget, and input gates are represented by f_t, i_t, C_t, and o_t, respectively. In addition, the weights and the biases assigned to these gates are b_f, w_f, and W_f; b_i, w_i, and W_i; b_c, w_c, and W_c; and b_o, w_o, and W_o. The GCRNN model combines RNNs and GCNs to capture the temporal and spatial features, with GCN layers extracting spatial data, LSTM layers modeling temporal aspects, and a dense layer producing the output.

E. Hyperparameter Tuning Method

Lastly, the hyperparameter tuning of the GCRNN approach was performed using the AO model [26]. The new population-based swarm intelligence optimizers, inspired by the aquila, a golden predatory bird known for its strength and speed in capturing prey like marmots and rabbits, form the basis of the AO model. This AO mimics the four different hunting methods and these methods are mathematically represented as:

1) Stage 1: Expanded Exploration (X_1)

During this phase, the aquila flies high above the ground level to properly scan the region before diving vertically after it has found the prey. This behavior is expressed as:

$$X_1(l+1) = X_B(l) * \left(1 - \frac{l}{L}\right) + (X_{mean}(l) - X_B(l) * rand) \quad (16)$$

$$X_{mean}(l) = \frac{1}{M}\sum_{i=1}^{M} X_i(l), \forall Mi = 1,2,\cdots,Dim \quad (17)$$

where $X_{mean}(l)$ denotes the mean position of the current solution at the i^{th} iteration using (17), X_B denotes the global best solution in this iteration, ran refers to randomly generated values and lies in $[0,1]$, l denotes the current iteration, L signifies the number of iterations, M denotes the size of the population, and Dim denotes the dimension size.

2) Stage2: Narrowed Exploration (X_2)

Most of aquila's hunting techniques involve this specific stage. Contour flying is combined with a brief slide to attack the prey. The subsequent equations constitute updates to the aquila locations:

$$X_2(l+1) = X_B(l) * Levy(D) + X_R(l) + (y - x) * rand \quad (18)$$

where X_R indicates aquila's random position, D represents the dimension space, and $Levy$ denotes the levy probability distribution function which is evaluated as:

$$Levy(D) = s * \frac{u * \sigma}{|v|^{\frac{1}{\beta}}} \quad (19)$$

$$\sigma = \frac{\Gamma(1+\beta) * sin\left(\frac{\pi\beta}{2}\right)}{\Gamma\left(\frac{1+\beta}{2}\right) * \beta * 2^{\frac{\beta-1}{2}}} \quad (20)$$

where s and β are constants with values of 0.01 and 1.5, respectively, and u and v are random numbers between the values of 0 and 1. The following two equations are used to calculate the values of x and y to model the spiral shape:

$$y = \gamma * cos(\theta) \quad (21)$$

$$x = \gamma * sin(\theta) \quad (22)$$

where θ and γ are determined by (23), (24), and (25):

$$\gamma = \gamma_1 + V * D_1 \quad (23)$$

$$\theta = -W * D_1 + \theta_1 \quad (24)$$

$$\theta_1 = \frac{3*\pi}{2} \quad (25)$$

where γ_1 takes a value between 1 and 20, V is equal to 0.0265, W is equit to 0.005, and D_1 represents the random integer from the range 1 to the dimension.

3) Stage3: Expanded Exploitation (X_3)

During this phase, the aquila focuses on locating the prey for a low-flying attack, with various attack modes available to the agents.

$$X_3(1+1) = \left(X_B(l) - X_{mean}(l)\right) * \alpha - rand + \left((\mathcal{UB} - \mathcal{LB}) * \text{rand} + \mathcal{LB}\right) * \delta \quad (26)$$

where α and δ are exploitation fixed parameters to 0.1, and $\mathcal{UB}$ and $\mathcal{LB}$ denote the upper and lower limits.

4) Stage4: Narrowed Exploitation (X_4)

The final stage involves the aquila's ability to quickly track and attack its prey using escape trajectory light, which is calculated as:

$$X_4(l+1) = QF * X_B(l) - (P_1 * X(l) * rand) - P_2 * Levy(D) + rand * P_1 \quad (27)$$

$$QF(l) = l^{\frac{2*rand-1}{(1-\gamma)^2}} \quad (28)$$

$$P_1 = 2 * rand - 1 \quad (29)$$

$$P_2 = 2 * \left(1 - \frac{l}{L}\right) \quad (30)$$

where $QF(l)$ denotes the quality value, P_1 represents the different motions of AO, and P_2 denotes the chasing target flight slope.

Fitness selection is a crucial feature that influences the performance of the AO approach. The hyperparameter selection process uses the solution encoder model to evaluate the efficiency of candidates, with the AO method prioritizing precision in its fitness function design.

$$Fitness = \max(P) \quad (31)$$

$$P = \frac{TP}{TP+FP} \quad (32)$$

where TP and FP represent the true and false positive values.

IV. PERFORMANCE ANALYSIS

In this section, the empirical validation of the OGCRNN-SBCRC approach is examined under the BC image dataset [27-29]. The suggested technique is simulated using the Python 3.6.5 tool on PC i5-8600k, 250GB SSD, GeForce 1050Ti 4GB, 16GB RAM, and 1TB HDD. The parameter settings are: learning rate: 0.01, activation: ReLU, epoch count: 50, dropout: 0.5, and batch size: 5. Table I shows the dataset description. An comparison between the OGCRNN-SBCRC methodology and recent techniques is displayed in Table II [30-33].

TABLE I. DETAILS OF THE DATASET

Class	No. of samples
Benign	2043
Malignant	1715
Total samples	3758

TABLE II. COMPARATIVE ANALYSIS OF OGCRNN-SBCRC METHOD WITH EXISTING MODELS [30-33]

Classifiers	Accuracy (%)	Precision (%)	Recall (%)	F1-score (%)
SVM [30]	93.81	96.97	94.06	92.15
LR [30]	96.41	98.05	97.52	98.60
NB [30]	94.73	98.60	96.90	91.99
EfficientNet-B3-ImageNet [31]	89.00	92.51	98.22	92.86
AlexNet-SVM [31]	91.00	95.64	95.65	97.22
AlexNet-DBN [31]	96.32	97.58	96.20	97.71
DenseNet201-ChexNet [31]	98.60	98.36	92.80	98.70
VGG+TL [32]	92.49	96.47	92.33	94.01
ResNet50 classifier [33]	98.00	94.24	93.09	93.53
NER SVM [33]	96.73	92.55	97.26	97.73
OGCRNN-SBCRC	99.65	99.59	99.69	99.64

The empirical results demonstrate that the performance of the OGCRNN-SBCRC method is superior to that of the other techniques. The OGCRNN-SBCRC method exhibited a superior Accuracy of 99.65% compared to the Support Vector Machine (SVM), Logistic Regression (LR), Naïve Bayes (NB), EfficientNet-B3-ImageNet, AlexNet-SVM, AlexNet-DBN, DenseNet201-ChexNet, VGG+TL, ResNet50, and NER SVM methods. Similarly, the OGCRNN-SBCRC method showed a superior Precision of 99.59% compared to the other techniques. Finally, it demonstrated the highest Recall and F1-score with values of 99.69% and 99.64%, respectively.

V. CONCLUSION

This study presents an Optimized Graph Convolutional Recurrent Neural Network based Segmentation for Breast Cancer Recognition and Classification (OGCRNN-SBCRC) technique using mammogram imaging. In the preprocessing phase, annotated images and masks are created and classified into benign and malignant categories. To achieve this, the OGCRNN-SBCRC technique employs a two-stage preprocessing approach: Wiener Filter (WF)-based noise removal and log transform-based contrast enhancement. The UNet++ and RMSProp optimizer are used for segmentation and parameter tuning. In addition, the ConvNeXtTiny Convolution Neural Network (CNN) model is utilized for extraction. The Graph Convolutional Recurrent Neural Network (GCRNN) model is employed for detection and classification. Finally, the hyperparameter tuning of the GCRNN approach is performed using the Aquila Optimizer (AO) model. The simulation analysis of the OGCRNN-SBCRC technique is performed implementing the Breast Cancer (BC) image dataset. The performance validation of the OGCRNN-SBCRC showed a superior accuracy value of 99.65% over the existing models. The limitations of the OGCRNN-SBCRC technique include the use of a limited dataset, which may affect the generalizability of the model. Future work may focus on expanding the dataset, enhancing robustness, and integrating interpretability tools for an improved clinical adoption.

REFERENCES

[1] Y. J. Tan, K. S. Sim, and F. F. Ting, "Breast cancer detection using convolutional neural networks for mammogram imaging system," in *2017 International Conference on Robotics, Automation and Sciences*, Melaka, Malaysia, 2017, pp. 1–5, https://doi.org/10.1109/ICORAS.2017.8308076.

[2] J. D. López-Cabrera, L. A. L. Rodríguez, and M. Pérez-Díaz, "Classification of Breast Cancer from Digital Mammography Using Deep Learning," *Inteligencia Artificial*, vol. 23, no. 65, pp. 56–66, May 2020, https://doi.org/10.4114/intartif.vol23iss65pp56-66.

[3] R. Vijayarajeswari, P. Parthasarathy, S. Vivekanandan, and A. A. Basha, "Classification of mammogram for early detection of breast cancer using SVM classifier and Hough transform," *Measurement*, vol. 146, pp. 800–805, Nov. 2019, https://doi.org/10.1016/j.measurement.2019.05.083.

[4] S. J. A. Sarosa, F. Utaminingrum, and F. A. Bachtiar, "Mammogram Breast Cancer Classification Using Gray-Level Co-Occurrence Matrix and Support Vector Machine," in *2018 International Conference on Sustainable Information Engineering and Technology*, Malang, Indonesia, 2018, pp. 54–59, https://doi.org/10.1109/SIET.2018.8693146.

[5] R. E. O. Torres, J. R. Gutiérrez, and A. G. L. Jacome, "Neutrosophic-based Machine Learning Techniques for Analysis and Diagnosis the Breast Cancer," *International Journal of Neutrosophic Science*, vol. 21, no. 1, pp. 162–173, May 2023, https://doi.org/10.54216/IJNS.210115.

[6] H. Nasir Khan, A. R. Shahid, B. Raza, A. H. Dar, and H. Alquhayz, "Multi-View Feature Fusion Based Four Views Model for Mammogram Classification Using Convolutional Neural Network," *IEEE Access*, vol. 7, pp. 165724–165733, Nov. 2019, https://doi.org/10.1109/ACCESS.2019.2953318.

[7] A. Bekkouche, M. Merzoug, M. Hadjila, and W. Ferhi, "Towards Early Breast Cancer Detection: A Deep Learning Approach," *Engineering, Technology & Applied Science Research*, vol. 14, no. 5, pp. 17517–17523, Oct. 2024, https://doi.org/10.48084/etasr.8634.

[8] S. M. Shaaban, M. Nawaz, Y. Said, and M. Barr, "An Efficient Breast Cancer Segmentation System based on Deep Learning Techniques," *Engineering, Technology & Applied Science Research*, vol. 13, no. 6, pp. 12415–12422, Dec. 2023, https://doi.org/10.48084/etasr.6518.

[9] R. Gurumoorthy and M. Kamarasan, "Breast Cancer Classification from Histopathological Images using Future Search Optimization Algorithm and Deep Learning," *Engineering, Technology & Applied Science Research*, vol. 14, no. 1, pp. 12831–12836, Feb. 2024, https://doi.org/10.48084/etasr.6720.

[10] A. Sahu, P. K. Das, and S. Meher, "An efficient deep learning scheme to detect breast cancer using mammogram and ultrasound breast images," *Biomedical Signal Processing and Control*, vol. 87, no. A, Jan. 2024, Art. no. 105377, https://doi.org/10.1016/j.bspc.2023.105377.

[11] L. Zaiter and R. Zwiggelaar, "Segmentation and classification of mammographic abnormalities using local binary patterns and deep learning," in *17th International Workshop on Breast Imaging*, Chicago, IL, USA, 2024, pp. 500–505, https://doi.org/10.1117/12.3026886.

[12] G. Meenalochini and S. Ramkumar, "A Deep Learning Based Breast Cancer Classification System Using Mammograms," *Journal of Electrical Engineering & Technology*, vol. 19, no. 4, pp. 2637–2650, May 2024, https://doi.org/10.1007/s42835-023-01747-x.

[13] V. Rathinam, R. Sasireka, and K. Valarmathi, "An Adaptive Fuzzy C-Means segmentation and deep learning model for efficient mammogram classification using VGG-Net," *Biomedical Signal Processing and Control*, vol. 88, no. B, Feb. 2024, Art. no. 105617, https://doi.org/10.1016/j.bspc.2023.105617.

[14] K. Jabeen *et al.*, "An intelligent healthcare framework for breast cancer diagnosis based on the information fusion of novel deep learning architectures and improved optimization algorithm," *Engineering Applications of Artificial Intelligence*, vol. 137, Nov. 2024, Art. no. 109152, https://doi.org/10.1016/j.engappai.2024.109152.

[15] L. Wang, "Mammography with deep learning for breast cancer detection," *Frontiers in Oncology*, vol. 14, Feb. 2024, Art. no. 1281922, https://doi.org/10.3389/fonc.2024.1281922.

[16] M. Khaled, F. Touazi, and D. Gaceb, "Improving Breast Cancer Diagnosis in Mammograms with Progressive Transfer Learning and Ensemble Deep Learning," *Arabian Journal for Science and Engineering*, Sep. 2024, https://doi.org/10.1007/s13369-024-09428-1.

[17] D. Lokhande and K. Rajeswari, "A Cloud-Based Breast Cancer Detection with Optimized Self-Attenuated Deep CNN," *International Journal of Image and Graphics*, Nov. 2024, Art. no. 2650039, https://doi.org/10.1142/S0219467826500397.

[18] K. Aguerchi, Y. Jabrane, M. Habba, and A. H. El Hassani, "A CNN Hyperparameters Optimization Based on Particle Swarm Optimization for Mammography Breast Cancer Classification," *Journal of Imaging*, vol. 10, no. 2, Feb. 2024, Art. no. 30, https://doi.org/10.3390/jimaging10020030.

[19] E. Asad, A. F. Mollah, S. Basu, and T. Chakraborti, "Deep features and metaheuristics guided optimization-based method for breast cancer diagnosis," *Multimedia Tools and Applications*, Jun. 2024, https://doi.org/10.1007/s11042-024-19629-3.

[20] N. Suganthi, S. Kotagiri, D. Thirupurasundari, and S. Vimala, "Adam golden search optimization enabled DCNN for classification of breast cancer using histopathological image," *Biomedical Signal Processing and Control*, vol. 94, Aug. 2024, Art. no. 106239, https://doi.org/10.1016/j.bspc.2024.106239.

[21] N. N. Ganvir and D. M. Yadav, "Filtering Method for Pre-processing Mammogram Images for Breast Cancer Detection," *International Journal of Engineering and Advanced Technology*, vol. 9, no. 1, pp. 4222–4229, Oct. 2019, https://doi.org/10.35940/ijeat.A1623.109119.

[22] S. Suresh, R. R. Madathil, C. S. Asha, and F. Dell'Acqua, "RDC-UNet++: An end-to-end network for multispectral satellite image enhancement," *Remote Sensing Applications: Society and Environment*, vol. 36, Nov. 2024, Art. no. 101293, https://doi.org/10.1016/j.rsase.2024.101293.

[23] S. M. Saqib *et al.*, "Lumpy skin disease diagnosis in cattle: A deep learning approach optimized with RMSProp and MobileNetV2," *Plos One*, vol. 19, no. 8, Aug. 2024, Art. no. e0302862, https://doi.org/10.1371/journal.pone.0302862.

[24] Y. Zhang, A. Xu, D. Lan, X. Zhang, J. Yin, and H. H. Goh, "ConvNeXt-based anchor-free object detection model for infrared image of power equipment," *Energy Reports*, vol. 9, no. 7, pp. 1121–1132, Sep. 2023, https://doi.org/10.1016/j.egyr.2023.04.145.

[25] A. Zanfei, B. M. Brentan, A. Menapace, M. Righetti, and M. Herrera, "Graph Convolutional Recurrent Neural Networks for Water Demand Forecasting," *Water Resources Research*, vol. 58, no. 7, Jul. 2022, Art. no. e2022WR032299, https://doi.org/10.1029/2022WR032299.

[26] S. Gopi and P. Mohapatra, "Fast random opposition-based learning Aquila optimization algorithm," *Heliyon*, vol. 10, no. 4, Feb. 2024, Art. no. e26187, https://doi.org/10.1016/j.heliyon.2024.e26187.

[27] "CBIS-DDSM: Breast Cancer Image Dataset." Kaggle, [Online]. Available: https://www.kaggle.com/datasets/awsaf49/cbis-ddsm-breast-cancer-image-dataset.

[28] R. Sawyer-Lee, F. Gimenez, A. Hoogi, and D. Rubin, "CBIS-DDSM | Curated Breast Imaging Subset of Digital Database for Screening Mammography." The Cancer Imaging Archive, 2016, https://doi.org/10.7937/K9/TCIA.2016.7O02S9CY.

[29] F. Villani, R. Civico, S. Pucci, L. Pizzimenti, R. Nappi, and P. M. De Martini, "A database of the coseismic effects following the 30 October 2016 Norcia earthquake in Central Italy," *Scientific Data*, vol. 5, no. 1, Mar. 2018, Art. no. 180049, https://doi.org/10.1038/sdata.2018.49.

[30] V. Jaiswal, P. Saurabh, U. K. Lilhore, M. Pathak, S. Simaiya, and S. Dalal, "A breast cancer risk predication and classification model with ensemble learning and big data fusion," *Decision Analytics Journal*, vol. 8, Sep. 2023, Art. no. 100298, https://doi.org/10.1016/j.dajour.2023.100298.

[31] R. Qasrawi *et al.*, "Hybrid ensemble deep learning model for advancing breast cancer detection and classification in clinical applications," *Heliyon*, vol. 10, no. 19, Oct. 2024, Art. no. e38374, https://doi.org/10.1016/j.heliyon.2024.e38374.

[32] Z. Liu, J. Peng, X. Guo, S. Chen, and L. Liu, "Breast cancer classification method based on improved VGG16 using mammography images," *Journal of Radiation Research and Applied Sciences*, vol. 17, no. 2, Jun. 2024, Art. no. 100885, https://doi.org/10.1016/j.jrras.2024.100885.

[33] S. Arooj *et al.*, "Data Fusion Architecture Empowered with Deep Learning for Breast Cancer Classification," *Computers, Materials & Continua*, vol. 77, no. 3, pp. 2813–2831, Dec. 2023, https://doi.org/10.32604/cmc.2023.043013.